The impact of water vapor on the OH reactivity toward CH₃CHO at ultra-low temperatures (21.7–135.0 K): Experiments and theory

Cite as: J. Chem. Phys. **155**, 034306 (2021); https://doi.org/10.1063/5.0054859 Submitted: 22 April 2021 • Accepted: 02 July 2021 • Published Online: 20 July 2021

🧓 E. M. Neeman, 🗓 D. González, 厄 S. Blázquez, et al.







ARTICLES YOU MAY BE INTERESTED IN

Nuclear-electronic orbital methods: Foundations and prospects
The Journal of Chemical Physics 155, 030901 (2021); https://doi.org/10.1063/5.0053576

The vacuum ultraviolet absorption spectrum of norbornadiene: Vibrational analysis of the singlet and triplet valence states of norbornadiene by configuration interaction and density functional calculations

The Journal of Chemical Physics 155, 034308 (2021); https://doi.org/10.1063/5.0053962

Quantum nature of molecular vibrational quenching: Water-molecular hydrogen collisions The Journal of Chemical Physics 155, 071104 (2021); https://doi.org/10.1063/5.0058755



Webinar
Quantum Material Characterization
for Streamlined Qubit Development



Register now



The impact of water vapor on the OH reactivity toward CH₃CHO at ultra-low temperatures (21.7-135.0 K): Experiments and theory

Cite as: J. Chem. Phys. 155, 034306 (2021); doi: 10.1063/5.0054859 Submitted: 22 April 2021 • Accepted: 2 July 2021 •







Published Online: 20 July 2021

E. M. Neeman, ^{1,a)} D. González, ¹ S. Blázquez, ¹ B. Ballesteros, ^{1,2} A. Canosa, ³ M. Antiñolo, ^{1,2,b)} D



L. Vereecken,^{4,c)} D J. Albaladejo,^{1,2} D and E. Jiménez^{1,2,c)} D



AFFILIATIONS

- Departamento de Química Física, Facultad de Ciencias y Tecnologías Químicas, Universidad de Castilla-La Mancha, Avda. Camilo José Cela 1B, 13071 Ciudad Real, Spain
- ²Instituto de Investigación en Combustión y Contaminación Atmosférica, Universidad de Castilla-La Mancha, Camino de Moledores s/n, 13071 Ciudad Real, Spain
- CNRS, IPR (Institut de Physique de Rennes)-UMR 6251, Université de Rennes, F-35000 Rennes, France
- ⁴Institute for Energy and Climate Research, IEK-8: Troposphere, Forschungszentrum Jülich GmbH, Jülich, Germany
- ^{a)}Current address: Univ. Lille, CNRS, UMR 8523-PhLAM-Physique des Lasers Atomes et Molécules, F-59000 Lille, France.
- b)Current address: Escuela de Ingeniería Industrial y Aeroespacial, Universidad de Castilla-La Mancha, Avenida Carlos III s/n, Real Fábrica de Armas, 45071 Toledo, Spain.
- ^{c)}Authors to whom correspondence should be addressed: L.Vereecken@fz-juelich.de and Elena.Jimenez@uclm.es

ABSTRACT

The role of water vapor (H₂O) and its hydrogen-bonded complexes in the gas-phase reactivity of organic compounds with hydroxyl (OH) radicals has been the subject of many recent studies. Contradictory effects have been reported at temperatures between 200 and 400 K. For the OH + acetaldehyde reaction, a slight catalytic effect of H₂O was previously reported at temperatures between 60 and 118 K. In this work, we used Laval nozzle expansions to reinvestigate the impact of H₂O on the OH-reactivity with acetaldehyde between 21.7 and 135.0 K. The results of this comprehensive study demonstrate that water, instead, slows down the reaction by factors of ~3 (21.7 K) and ~2 (36.2-89.5 K), and almost no effect of added H2O was observed at 135.0 K.

Published under an exclusive license by AIP Publishing. https://doi.org/10.1063/5.0054859

I. INTRODUCTION

Water vapor, H₂O, is one of the most abundant species in the Earth's atmosphere (up to 4% in the troposphere, T = 220-298 K). One of the most relevant processes involving H2O in our atmosphere is the formation of the main diurnal oxidant, the hydroxyl (OH) radical, which acts as a major sink for many species. Water has also been found in the atmosphere of many objects in the solar system at low temperature conditions ($T \le 150$ K), such as Europa, one of Jupiter's moons, and Enceladus² or Titan,³ both orbiting Saturn. Furthermore, in comets and lower temperature environments, such as the interstellar medium, H₂O⁴⁻⁶ and OH radicals⁷⁻⁹ and some organics, such as acetaldehyde (CH₃CHO), ¹⁰⁻¹³ were also detected. The effect of water vapor on the kinetics of the OH

reactions with some organic compounds at temperatures of interest for the Earth's atmosphere has been investigated mainly by theoretical calculations. 14-21 In those studies, the predicted effect of water on the OH-reactivity varies depending on the organic molecule or the theoretical method used. This is demonstrated in Table I, which summarizes the investigated OH reactions to date. The ratio of the rate coefficients in the presence of water $[k_{water}(T)]$ to the one in the absence of water $[k_{no \text{ water}}(T)]$ is given in Table I. Changes by many orders of magnitude according to the reactant of concern can be observed. For example, in the case of ethanol, the theoretical work¹⁹ predicts a decrease in the effective OH-rate coefficient for the monohydrated and dehydrated reaction patterns compared to a non-hydrated reaction. It has been found that the effective rate coefficients of the corresponding monohydrated reactions are 3-4

TABLE I. Summary of the theoretical works on some OH reactions in the presence of H₂O.

Organics	T (K)	Water complex reaction	$k_{\text{water}}(T)/k_{\text{no_water}}(T)$	References
CH ₄	298	$OH(H_2O) + CH_4$	4.3×10^{-3}	Allodi <i>et al.</i> ¹⁸
CH ₃ CH ₂ OH	298.2 216.7	$OH(H_2O) + CH_3CH_2OH$ $OH(H_2O) + CH_3CH_2OH$	$1.1 \times 10^{-3} \\ 1.4 \times 10^{-4}$	Xu et al. ¹⁹ Xu et al. ¹⁹
HC(O)OH	298 298	$OH(H_2O) + HC(O)OH$ $OH + HC(O)OH(H_2O)$	0.69 0.27	Anglada and Gonzalez ¹⁴ Anglada and Gonzalez ¹⁴
CH ₃ C(O)CH ₃	298 220	$OH + CH_3C(O)CH_3(H_2O)$ $OH + CH_3C(O)CH_3(H_2O)$		Iuga et al. ¹⁶ Iuga et al. ¹⁶
(HCO) ₂	298	$OH + (HCO)_2(H_2O)$	8×10^{-4}	Iuga et al. ¹⁵
CH₃CHO	298 220	$OH + CH_3CHO(H_2O)$	5.3×10^{-4} 0.22	Iuga et al. ¹⁷ Iuga et al. ¹⁷
CH ₃ OH	298 298 200–400	$CH_3OH + OH + H_2O$ $CH_3OH + OH + 2H_2O$ $OH(CH_3OH) + H_2O$	2.96×10^{-3} 5.81×10^{-4} ~ 1.0	Chao et al. ²⁰ Chao et al. ²⁰ Wu et al. ²¹

orders of magnitude lower than those of the non-hydrated reaction, indicating that water has a decelerating effect on the studied reaction. Several mechanisms have been considered, including hydration of either the OH radical or the organic reactant and formation of an adduct in the specific case of methanol. Interestingly, the extent of the computed decrease in k(T) is somewhat different for HC(O)OH depending on the water complex formed, OH(H₂O) or HC(O)OH(H₂O). For CH₃C(O)CH₃, (HCO)₂, and CH₃CHO, only hydration of the organic reactant that further reacts with OH radicals has been suggested. ^{15–17,22} In the specific case of acetaldehyde, Iuga *et al.* ¹⁷ computed that $k_{\text{water}}(T)$ is several orders of magnitude lower than $k_{\text{no_water}}(T)$ at 298 K. Furthermore, their calculation at 220 K indicates a significant increase in the $k_{\text{water}}(T)/k_{\text{no_water}}(T)$ ratio.

Experimentally, the investigation of the role of water vapor on OH removal is very scarce and also contradictory. As far as we know, only for saturated alcohols $^{20,23-25}$ and aldehydes, 22,26 the effect of water vapor on the measured OH-rate coefficient, $k_{\rm obs}({\rm T})$, has been reported. At room temperature, Jara-Toro et~al. reported, at a relative humidity (RH) between 20% and 95%, a slight increase in $k_{\rm obs}({\rm T})$ for the OH reactions of methanol, 23 ethanol, and n-propanol 24 with respect to those measured in the absence of added ${\rm H_2O}$. This was rebated, however, for methanol and ethanol by Chao $et~al.^{20}$ and Weber $et~al.^{25}$ respectively, who did not observe any catalytic effect of ${\rm H_2O}$ at similar RHs.

Vöhringer-Martinez *et al.* also reported a non-catalytic effect of $\rm H_2O$ for $\rm CH_3CHO^{22}$ and propanal 26 at 298 K. In contrast, these authors observed that $k_{\rm obs}(\rm T)$ at 60 K increases about twice in the presence of about 3% of $\rm H_2O$ in the case of $\rm CH_3CHO$. To support their experimental observation, Vöhringer-Martinez *et al.* 22 performed a quantum chemical study finding that the complexation in $\rm CH_3CHO(H_2O)$ opens an additional channel for OH removal with an energetically more favorable submerged reaction barrier than in the absence of water. However, no theory-based rate coefficients were reported.

Smith²⁷ suggested that new experimental and theoretical works are required to understand the effect of water on chemical kinetics at temperatures lower than 60 K. Therefore, in this study, we address the challenging and interesting questions: how does water influence the OH-reactivity toward CH₃CHO? Is water a real active catalyst as it has been proposed previously?²² For this purpose, herein, we report a comprehensive experimental kinetic study of the gas-phase OH removal in the presence of CH₃CHO, both in the absence and in the presence of water between 21.7 and 135.0 K. To compare against the previous work from Vöhringer-Martinez *et al.*,²² we carried out the kinetic experiments under similar conditions of gas temperature and pressure and also extended our investigations down to ~20 K. In addition, quantum chemical calculations that support the obtained results are also presented.

II. EXPERIMENTAL TECHNIQUE

A. CRESU apparatus coupled to pulsed laser photolysis-laser induced fluorescence (PLP-LIF) technique

The kinetic experiments of the OH removal by a reaction with CH_3CHO in the presence and absence of water were performed using the pulsed Reaction Kinetics in Uniform Supersonic Flows (CRESU) machine built in the Department of Physical Chemistry (University of Castilla-La Mancha) in Ciudad Real (Spain). The apparatus and technique were described in detail elsewhere²⁸ and are only briefly discussed here.

The principle of this technique is to use a carrier gas flow, containing small mixing ratios of OH-precursor (H_2O_2) and coreactants (CH₃CHO and H₂O) expanded from a high-pressure reservoir to a low-pressure chamber through a pulsed convergent-divergent nozzle (Laval-type). During the expansion, an isentropic core is generated in the jet, where its velocity, temperature, and density (n) are essentially constant throughout many tens of centimeters

from the exit of the Laval nozzle. The time corresponding to the optimal length of uniformity, usually called *hydrodynamic time*, t_{hydro} , is dependent on the Laval nozzle geometry and the flow conditions expanding through.

Electronic ground state OH radicals, $OH(X^2\Pi)$, were generated *in situ* in the jet by pulsed laser photolysis (PLP) of gaseous H_2O_2 at 248 nm using a KrF excimer laser. The loss of $OH(X^2\Pi)$ in the time scale provided by the hydrodynamic time (t_{hydro}) was monitored by exciting the $OH(^2\Pi, v''=0) \rightarrow OH(^2\Sigma, v'=1)$ transition at ~282 nm doubled the output of a dye laser (Lambda Physik, model Scanmate) pumped by the second harmonic of a Nd:YAG laser (Continuum, model Surelite) and by subsequently collecting its laser induced fluorescence (LIF) at ~310 nm $OH(^2\Sigma, v'=0) \rightarrow OH(^2\Pi, v''=0)$ with a filtered photomultiplier tube (PMT) (Electron Tube, model 9813B). The PMT signal was sent to a gated boxcar integration unit (Stanford Research System, model SRS250). The integrated signal was treated and recorded by a homemade LabView program.

The kinetic experiments were carried out under *pseudo*-first-order conditions, i.e., the initial concentrations of CH_3CHO , H_2O , and H_2O_2 in the supersonic jet ([$CH_3CHO]_0$, [$H_2O]_0$, and [$H_2O_2]_0$) were in large excess with respect to [$OH]_0$. Under these conditions, from the analysis of the exponential OH LIF signal (I_{LIF}) decays after rotational relaxation of OH, the *pseudo*-first-order rate coefficients, k', were obtained as a function of [$CH_3CHO]_0$ and a well-known quantity of water in the jet. In Fig. 1, examples of the OH LIF temporal profiles are presented for the lowest and highest temperature of this work, i.e., 21.7 and 135.0 K. In Figs. 1(a) and 1(b), the OH temporal profiles were obtained either in the absence of CH_3CHO and H_2O (red decays) or in the presence of only H_2O (black decays) or finally in the presence of both CH_3CHO and H_2O (the same concentration as for the black curve) (blue decays).

B. Liquid and gas handling

The main carrier gas (He, N_2 , or a binary mixture of them, ²⁹ 80% N_2 + 20% He) was introduced in the reservoir using a calibrated mass flow controller (Sierra Instruments, Inc., models: Smart-Trak 2 and Smart-Trak 100).

Since the OH-precursor (H_2O_2) and water are liquids in the laboratory conditions, to introduce them into the reservoir of the CRESU reactor, a controlled flow of carrier gas was passed through independent glass bubblers containing a pre-concentrated commercial aqueous solution of $H_2O_2^{30,31}$ and ultra-purity H_2O , respectively (see Scheme 1). These bubblers were submerged in a water bath to keep liquid H_2O_2 and H_2O at room temperature, thus ensuring a constant vapor pressure. For H_2O , two different bubblers were used: one with a porous diffuser for small carrier gas flows (lower than 0.35 slpm) and the other one without a diffuser for higher gas flows (higher than 0.35 slpm).

Acetaldehyde is also liquid in the usual laboratory conditions. The sample is degassed with several freeze–pump–thaw cycles before every use. Since its vapor pressure at room temperature is significant (1200 mbar at 25 $^{\circ}$ C), it was easily evaporated from a round flask (V = 250 ml) connected to a vacuum line into a 50-L glass bulb preliminary pumped under vacuum. The pressure (P_{CH₃CHO}) introduced in the 50-L storage bulb was measured acetaldehyde partial

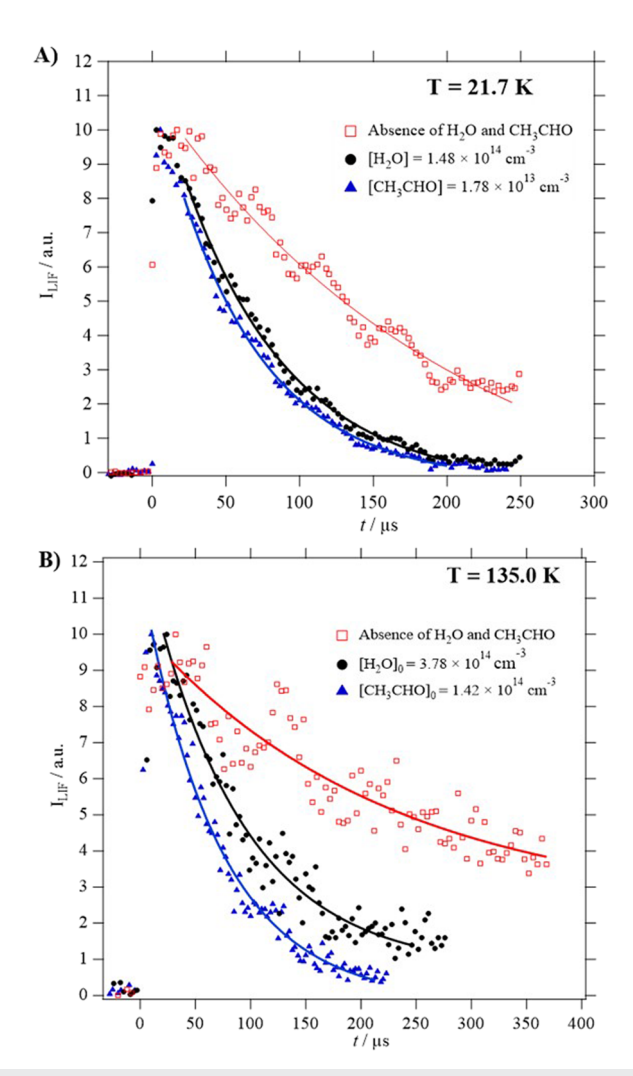
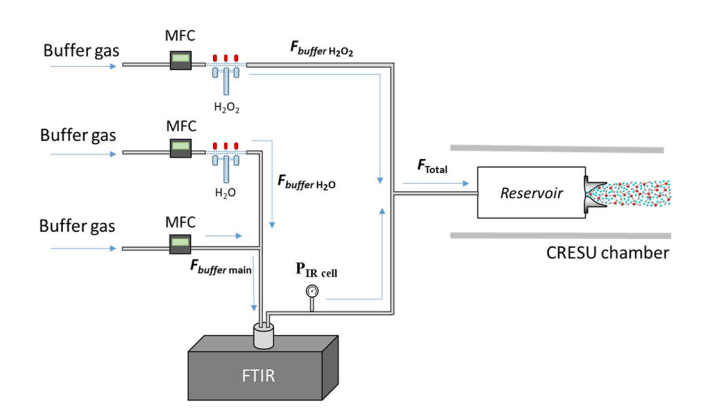


FIG. 1. LIF profiles of OH radicals registered at (a) 21.7 K and (b) 135.0 K in the absence of CH_3CHO and H_2O (red decays), in the presence of only H_2O (black decays), and in the presence of both CH_3CHO and H_2O (the same concentration as in the black curve) (blue decays).

with a pressure gauge (Ceravac CTR 100N from Leybold). The bulb was filled up to about 1 bar of carrier gas (P_T). The dilution factor $f_{\rm CH_3CHO}$ is then obtained as the $P_{\rm CH_3CHO}/P_T$ ratio. Since a precise knowledge of the acetaldehyde and water concentrations is crucial in the determination of the rate coefficients, a careful protocol has been established for both reactants. This is discussed in Secs. II C and II D.

C. Measurement of gas-phase CH₃CHO concentrations

The acetaldehyde concentration in the jet, $[CH_3CHO]_0$, was varied by changing the mass flow rate (F_{CH_3CHO}) of the diluted acetaldehyde set in the storage bulb and maintaining the total mass flow rate (F_{Total}) constant. To calculate $[CH_3CHO]_0$, all mass flow



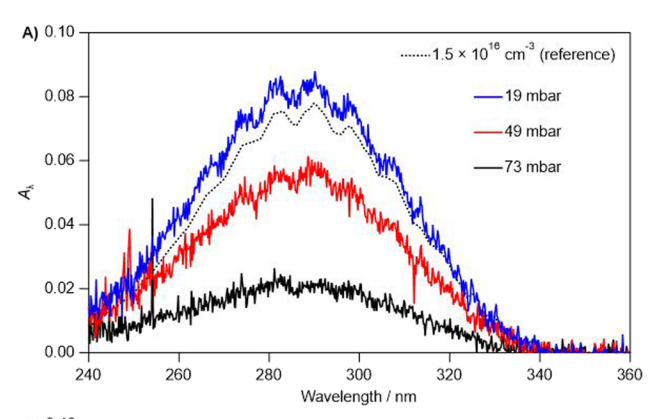
SCHEME 1. Schematic illustration of the gas flows (blue arrows) introduced in the FTIR to measure the water concentration before entering the *reservoir*. **MFC**: mass flow controller.

rates (F_i) , the dilution factor $f_{\text{CH}_3\text{CHO}}$ in the storage bulb, and the total gas density n provided by Pitot tube measurements are considered,

$$[CH3CHO]0 = \frac{F_{CH3CHO}}{F_{Total}} n f_{CH3CHO}.$$
 (I)

 F_{Total} is the sum of all flow rates: the main flow of the buffer gas ($F_{\mathrm{buffer\ main}}$), the buffer gas flows through the H₂O ($F_{\mathrm{buffer\ H_2O}}$) and H₂O₂ ($F_{\mathrm{buffer\ H_2O}}$) glass bubblers, and $F_{\mathrm{CH_3CHO}}$ (see Table II).

The values of f_{CH_3CHO} were checked offline by measuring the CH₃CHO concentration in the storage bulb by UV spectroscopy between 240 and 360 nm, as explained by Blázquez et al.32 In Fig. 2(a), an example of the recorded UV spectra [absorbance in base $e(A_{\lambda})$ vs wavelength λ] from diluted CH₃CHO from the storage bulb is shown at different total pressures together with a reference CH₃CHO spectrum built using a concentration of 1.5×10^{16} molecules cm⁻³, the optical path length (107 cm), and the absorption cross sections recommended by Jet Propulsion Laboratory.33 The experimental UV system used was described previously. 32,34-37 A 30 W deuterium lamp (Oriel, model: Q Series Low Power) was used to irradiate the gas mixture in the absorption cell. The transmitted light was focused on a 0.5 m spectrometer (Chromex 500 is/ms), which has a grating (300 groves per mm with a spectral resolution of 0.19 nm) that disperses the radiation. The dispersed light was detected with a cooled CCD detector (Andor, model: DB401-UV, $1024 \times 128 \text{ pixel}^2$).



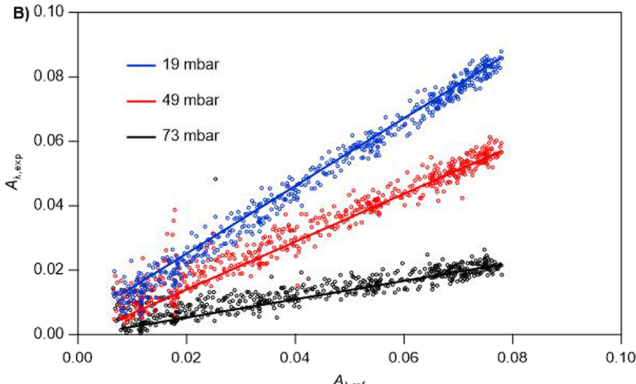


FIG. 2. (a) Examples of the UV spectrum of samples from the storage bulb at three different total pressures in the UV cell ($P_{UV,cell}$). (b) Plots of Eq. (II) for the data presented in (a).

As shown in Fig. 2(b), $f_{\text{CH}_3\text{CHO}}$ can be obtained considering the ratio between the experimental and reference spectra given in the following equation:

$$\frac{A_{\lambda,exp}}{A_{\lambda,ref}} = \frac{[CH_3CHO]_{exp}}{[CH_3CHO]_{ref}},$$
 (II)

where [CH₃CHO]_{exp} is given as follows:

$$[CH3CHO]_{exp} = f_{CH3CHO} \frac{P_{UV cell}}{RT}.$$
 (III)

TABLE II. Calibrated flow rates introduced in the pre-expansion chamber.^a

T (K)	F _{buffer main} /slpm	F _{buffer H₂O} /slpm	F _{buffer H₂O₂/slpm}	F _{CH₃CHO} /sccm	F _{Total} /slpm
21.7 ± 1.4	8.6-12.7	0.04-0.76	0.077	15.1-237	9.3-12.9
36.2 ± 1.2	7.4-12.3	0.58 - 4.6	0.048 - 0.059	24.4-102	12.1-13.2
64.1 ± 1.2	1.1-1.9	0.094 - 0.66	0.010 - 0.023	7.4-143	1.30 - 1.90
89.5 ± 1.2	4.0-5.6	1.27 - 2.82	0.020 - 0.038	31.3-165	1.30 - 1.90
135.0 ± 0.8	4.4-8.2	0.65-2.82	0.029	7.3-130	5.70-8.20

^aIn standard liters per minute (slpm) or standard cubic centimeters per minute (sccm).

Then, [CH₃CHO]_{exp} is determined from the slope of the absorbance $A_{\lambda,exp}$ vs the reference absorbance $A_{\lambda,ref}$ plots and P_{UVcell} is the total pressure in the UV cell $[P_{UVcell} = 19-73 \text{ mbar}]$ in the example in Fig. 2(b)]. The measured mixing ratios $f_{\text{CH}_3\text{CHO}}$ from UV measurements agreed with those obtained from pressure measurements $(9 \times 10^{-3} - 4.7 \times 10^{-2})$ with differences less than 6% between $f_{\text{CH}_3\text{CHO}}$.

D. Spectroscopic measurement of H₂O concentrations

The initial water concentration was spectroscopically measured online before the supersonic expansion (i.e., at room temperature) by using a Fourier Transform Infrared (FTIR) spectrometer described earlier.^{36,38} For this, the main flow of the buffer gas seeded with gaseous H2O, coming from the glass bubbler, was introduced into an IR cell placed upstream of the CRESU reservoir (see Scheme 1). This cell is a multipass one (Specac, model Cyclone C5) sealed by ZnSe windows.^{36,38} The optical path length was set to 800 cm. The total pressure in the IR cell (PIR cell) was between 215 and 600 mbar. The IR spectrum of diluted H_2O was recorded between 500 and 4000 cm⁻¹ using a FTIR spectrometer (Bruker, model Tensor 27) with a Globar lamp and a mercury cadmium telluride (MCT) detector cooled by liquid nitrogen.

The followed procedure is given as follows:

- Once the IR spectrum of diluted H₂O was recorded, the MALT^{39,40} (Multiple Atmospheric Layer Transmission) software was used to retrieve the mole fraction of H₂O vapor in the gas flow before the supersonic expansion, $x(H_2O)_{IR cell}$.
- Neglecting the H₂O₂/buffer gas flow directly introduced in the reservoir, the water concentration in the cooled jet, [H₂O]₀, can be deduced by simply multiplying the total gas density of the jet (*n*) by $x(H_2O)_{IR cell}$.

MALT uses a non-linear least-squares spectral fitting computational procedure developed by Griffith.⁴⁰ This method simulates the spectrum of the mixture from a set of initial concentrations and then varies the concentrations iteratively to minimize the residual between the measured and simulated spectra. MALT takes the line parameters (positions, strengths, widths, and the temperature dependences for each absorption line) from HITRAN08⁴¹ database to generate a reference spectrum, considering the experimental conditions, such as temperature (298 K), P_{IR cell}, and path length (800 cm) of the IR cell and the instrumental resolution of the IR spectrometer (1 cm⁻¹). An iterative procedure is applied to obtain the best match to the experimental spectra and to yield the mole fraction of H₂O in the IR cell.

III. THEORETICAL METHODOLOGY

The geometries of the molecules studied were optimized at the M06-2X-D3/aug-cc-pVTZ level of theory, 42-44 where the inclusion of diffuse orbitals and Grimme D3 dispersion correction^{44,45} specifically aims to provide a good description even for the longdistance interactions in the complexes. To further improve the relative energies, single point coupled-cluster single double triple [CCSD(T)]/aug-cc-pVTZ energy calculations were performed,⁴⁶ which were combined with zero-point energy corrections at the

M06-2X-D3 level of theory (wavenumber scaling 0.971).⁴⁷ It was attempted to exhaustively characterize all conformers for the CH₃CHO + OH, CH₃CHO + H₂O, CH₃CHO + H₂O + OH, CH₃CHO + CH₃CHO, and CH₃CO + H₂O complexes.

This was done by generating a large number of starting geometries (200-400) at a moderate distance of the pertaining agents for each complex, spanning the entire (half)sphere of the approach vectors and for each approach a set of different relative rotations of the constituents. These initial geometries were allowed to relax in M06-2X/cc-pVDZ energy minimization calculations, initiated with an explicit Hessian calculation to get an optimal start of the downhill trajectory. The resulting minimum geometries were then further optimized at the M06-2X-D3/aug-cc-pVTZ level of theory. Equilibrium constants for these complexes were calculated at the high-pressure limit based on the ratio of the temperaturedependent partition functions and the aforementioned ZPEcorrected relative energies using the rigid rotor harmonic oscillator approximation.

Semi-quantitative theoretical kinetic calculations were performed based on equilibrium constants, transition state theory, and Rice-Ramsperger-Kassel-Marcus (RRKM) theory;⁴⁸⁻⁵¹ the relevant formulas are given below. All these calculations were performed in a rigid rotor harmonic oscillator approximation. The quantum chemical calculations were done using the Gaussian16 program suite.⁵² The thermodynamic and kinetic calculations were performed using in-house software.

IV. EXPERIMENTAL RESULTS AND DISCUSSION

A. Determination of the onset for CH₂CHO dimerization at ultralow temperatures

It is recognized for a long time that the clustering process is enhanced and favored at low temperatures. The first step of a clustering process, the dimerization, has widely been discussed in the literature for different organic compounds. 31,32,53 At the ultralow temperatures of the present work, the formation of (CH₃CHO)₂ may occur in the time scale of the kinetic experiments when high initial concentrations of CH₃CHO are introduced in the CRESU chamber,

$$CH_3CHO + CH_3CHO \rightarrow (CH_3CHO)_2$$
 k_{dimer} . (1)

Since reaction (1) reduces the amount of "free" acetaldehyde in the cooled jet, the measured rate coefficient can be underestimated. 32,3 For that reason, at first, kinetic studies are performed without added water in a wide concentration range of [CH₃CHO]₀ in order to identify the threshold of dimerization, which means the acetaldehyde concentration beyond which the pseudo-first-order plots start to present a clear downward curvature (see Fig. 3 as an example at 21.7 K). To compare different experiments at the same temperature, $k' - k'_0$ is plotted vs[CH₃CHO]₀ using the following equation:

$$\mathbf{k}' - \mathbf{k}'_0 = \mathbf{k}_{obs}(\mathbf{T})[CH_3CHO]_0,$$
 (IV)

where k'_0 is k' obtained in the absence of CH₃CHO at a constant

Once the threshold of dimerization is identified, all kinetic experiments without added water at a given temperature were car-

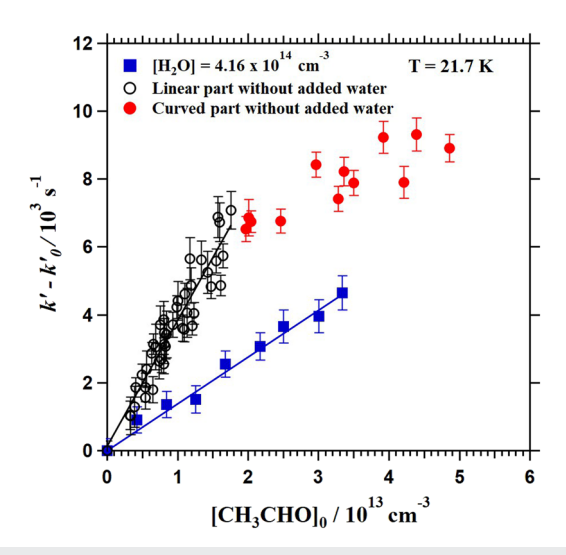


FIG. 3. Examples of the corrected pseudo-first-order rate coefficients, $k'-k'_0$, as a function of initial acetaldehyde concentration without and with added H₂O (4.16 \times 10¹⁴ cm⁻³) at 21.7 K.

ried out in the linear part of the $k' - k'_0$ vs $[CH_3CHO]_0$ plots to ensure that the dimerization process is negligible and not affecting the measured k(T).

As shown in Fig. 3, the red circles correspond to the kinetic data in the curved zone, where dimerization occurs, and they were disregarded in the kinetic analysis. In the presence of water, no downward curvature of $k'-k'_0$ vs $[CH_3CHO]_0$ plots was observed in the same concentration range and beyond (as shown in Fig. 3 for T = 21.7 K). That means that much higher (more than twice at 21.7 K) initial concentrations of CH_3CHO can be added when water is present and the $k'-k'_0$ vs concentration plots remain linear. Our experimental observations of the effect of H_2O on the $(CH_3CHO)_2$ formation are in good agreement with the theoretical results (see Fig. 8 and Fig. S1), which indicate that the water complex, $CH_3CHO(H_2O)$, is sufficiently stable to evacuate CH_3CHO from its dimer complexes if any are present as in the experiment of Vöhringer-Martinez *et al.*

B. Effect of H_2O on the observed rate coefficient, $k_{obs}(T)$, as a function of temperature

As exemplified in Fig. 4 for selected temperatures, $k' - k'_0$ is linearly correlated with $[CH_3CHO]_0$, both in the absence and in the presence of a constant $[H_2O]_0$, as reflected by using Eq. (IV). As can be deduced from the slopes of the plots presented in Fig. 4 and summarized in Table III, $k_{\rm obs}(T)$ decreases in the presence of H_2O , making the OH-reactivity slower. In Table III, the uncertainties in $k_{\rm obs}(T)$ are statistical $\pm 2\sigma$, while uncertainties in k'_0 are statistical $\pm 1\sigma$. The systematic errors in $k_{\rm obs}(T)$ are mainly related with inaccuracies or miscalibrations of instruments, such as mass flow controllers or pressure gauges, which directly affect the determination of the acetaldehyde concentration. Based on the typical differences (6%) between the mass flow and optical measurements of $[CH_3CHO]_0$, a conservative 10% systematic error can be added to the statistical uncertainties. In the absence of added H_2O , $k_{\rm obs}(T)$ are in agreement with those previously reported by Blázquez *et al.*³² for

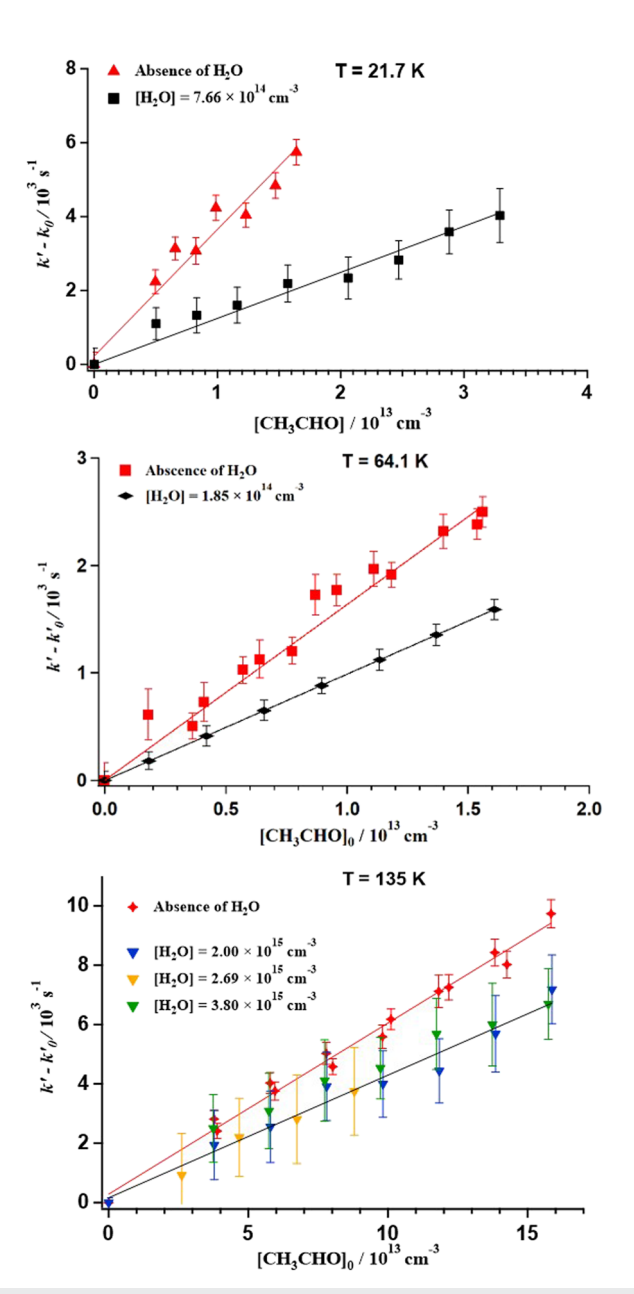


FIG. 4. Examples of the corrected pseudo-first-order rate coefficients, $k'-k'_0$, as a function of the initial acetaldehyde concentration with and without added H₂O at 21.7, 64.1, and 135.0 K. Uncertainties are $\pm 1\sigma$.

the OH + CH₃CHO reaction [k(T)] at ultralow temperatures. At the highest temperature, 135 K, however, a slightly higher $k_{\rm obs}(T)$ was found in the present investigation.

In the presence of a large excess of H_2O , $k_{obs}(T)$ drastically decreases in the 21.7–89.5 K range with respect to those measured without added water, while at 135.0 K, $k_{obs}(T)$ is not affected by $[H_2O]_0$, within the experimental uncertainties, confirming that at high temperatures, the OH + CH₃CHO reaction is not water-assisted. These observations are contradictory to those pre-

TABLE III. Initial concentrations of added H_2O , CH_3CHO , and the observed rate coefficients in the absence ($\emph{K'}_0$) and in the presence of CH_3CHO ($\emph{K}_{obs}(T)$) as a function of temperature.

T (K)	$[H_2O]_0$ (10 ¹⁴ molecules cm ⁻³)	$[CH_3CHO]_0$ (10 ¹³ molecules cm ⁻³)	$k'_0 \pm 1\sigma$ (s^{-1})	$k_{\rm obs}({\rm T}) \pm 2\sigma$ (10 ⁻¹⁰ cm ³ s ⁻¹)
	0	0.33-1.80	5 307 ± 235	3.69 ± 0.44
	0.10	0.81-3.64	8791 ± 274	3.42 ± 0.30
	0.13	0.72-3.56	6989 ± 223	3.31 ± 0.44
	0.15	0.71-3.57	6855 ± 227	2.86 ± 0.46
	0.33	0.34-3.53	8410 ± 259	3.17 ± 0.49
	0.50	0.76-3.00	8830 ± 241	2.34 ± 0.18
	0.59	0.36-3.49	8884 ± 279	2.77 ± 0.70
21.7 ± 1.4	0.67	0.36-3.54	10571 ± 273	2.77 ± 0.70 2.71 ± 0.60
	0.82	0.55-3.57	10371 ± 273 10881 ± 237	2.47 ± 0.36
	1.48	0.41-1.78	10161 ± 257 10161 ± 361	1.73 ± 0.14
			16843 ± 120	
	2.80	0.40-1.97		1.38 ± 0.12
	4.16	0.42-3.33	15063 ± 180	1.34 ± 0.12
	7.56	0.77-3.06	19083 ± 236	1.30 ± 0.19
	7.67	0.50-3.29	16898 ± 218	1.12 ± 0.13
	0	0.34-3.83	7447 ± 147	2.18 ± 0.16
	0.36	2.01-4.08	17083 ± 411	1.56 ± 0.19
	0.46	1.16-4.24	14078 ± 259	2.14 ± 0.18
	0.71	2.01-4.08	19880 ± 716	1.47 ± 0.26
	0.89	2.08-4.21	18073 ± 856	1.17 ± 0.11
36.2 ± 1.2	1.06	1.16-4.68	19564 ± 294	1.12 ± 0.26
	1.94	1.63-4.76	24620 ± 657	1.27 ± 0.12
	2.13	2.09-4.66	24062 ± 788	1.01 ± 0.25
	3.07	2.48-4.17	27314 ± 771	0.95 ± 0.12
	3.55	2.11-5.15	25324 ± 1000	0.97 ± 0.12
	4.24	1.67-3.97	28478 ± 893	0.85 ± 0.55
	0	0.17-3.05	2 812 ± 62	1.45 ± 0.14
	1.85	0.18-1.59	8708 ± 81	0.94 ± 0.10
	5.84	0.18-1.61	10928 ± 100	0.86 ± 0.37
	8.17	0.18-1.56	11314 ± 220	0.79 ± 0.13
64.1 ± 1.6	11.5	0.18-1.61	12790 ± 197	0.86 ± 0.12
	13.7	0.18-1.58	13798 ± 410	0.79 ± 0.06
	16.7	0.19-1.64	15736 ± 307 15526 ± 307	0.64 ± 0.10
	22.4	0.18–1.61	14720 ± 576	0.64 ± 0.14
	0	0.41-3.96	3.054 ± 74	0.85 ± 0.06
00.5 . 0.6	11.5	0.80-4.21	10523 ± 605	0.60 ± 0.20
89.5 ± 0.6	14.2	0.80-4.23	14018 ± 735	0.53 ± 0.08
	22.3	0.80-4.21	15897 ± 894	0.50 ± 0.11
	29.4	0.79-4.21	17649 ± 743	0.47 ± 0.11
	0	1.66-16.4	2661 ± 188	0.58 ± 0.04
135.0 ± 0.8	3.77	3.86-16.2	8889 ± 337	0.42 ± 0.10
	10.5	3.81-16.0	15749 ± 670	0.41 ± 0.08
	20.0	3.78-15.9	17517 ± 566	0.41 ± 0.06
	26.9	2.61-8.79	22558 ± 53	0.43 ± 0.05
	28.6	1.58-13.0	31048 ± 702	0.34 ± 0.03
	38.0	3.75-15.7	17473 ± 532	0.41 ± 0.06

viously reported by Vöhringer-Martinez *et al.*, ²² who observed an increase, about a factor of two, of $k_{\rm obs}(60{\text -}118~{\rm K})$ in the presence of about 3% H₂O in the gas flow (i.e., [H₂O]₀ = 1.5 × 10¹⁵ cm⁻³ at 60 K and 3.3 × 10¹⁵ cm⁻³ at 118 K). A potential reason for the

discrepancy with the experiments of Vöhringer-Martinez *et al.* is a direct consequence of the *short time scale* used by these authors (e.g., $80~\mu s$ at 77 K). To observe a decay of the LIF signal over several OH-lifetimes in that time scale, *high initial concentrations* of

acetaldehyde are needed. Their concentration range is more than 5 times higher than that used in this work. Employing high $[CH_3CHO]_0$, especially in the experiments without added H_2O , provokes the formation of acetaldehyde dimers, $(CH_3CHO)_2$, as shown in Fig. 3 and discussed also by Blázquez *et al.*, ³² yielding curved k' (or $k' - k'_0$) vs $[CH_3CHO]_0$ plots and a lower slope, implying a lower $k_{\rm obs}(T)$ when fitted to a straight line according to Eq. (II). Blázquez *et al.* ³² showed evidences that $k_{\rm obs}(T)$ obtained by Vöhringer-Martinez *et al.*, in the absence of water, were underestimated for that reason.

As mentioned above, the use of low $[CH_3CHO]_0$ ensures us to perform the kinetic study below the onset of acetaldehyde dimerization. As can be seen in Fig. 5, $k_{obs}(T)$ reaches a roughly constant value at a certain $[H_2O]_0$. When $[H_2O] \rightarrow \infty$, all CH_3CHO is converted into the $CH_3CHO(H_2O)$ complex [reaction (2)] and then the OH loss is dominated by reaction (3) in this limit condition,

$$H_2O + CH_3CHO \rightarrow CH_3CHO(H_2O)$$
 $k_{complex}(T)$, (2)

$$OH + CH_3CHO(H_2O) \rightarrow 2H_2O + CH_3C(O)$$
 $k_{OH_complex}(T)$. (3

To physically interpret the observed dependence of $k_{\rm obs}(T)$ with the water content, the time-dependence of [CH₃CHO] and [CH₃CHO(H₂O)] has to be taken into account to derive $k' - k'_0$ and to further compare with Eq. (IV). From the rate equation expressed as the OH loss by a reaction with CH₃CHO and CH₃CHO(H₂O), $k' - k'_0$ is given by

$$k' - k'_0 = k(T)[CH_3CHO]$$

+ $k_{OH_complex}(T)[CH_3CHO(H_2O)].$ (V)

In the presence of an excess of water, the destruction of acetaldehyde is essentially due to the association process [reaction (2)] with a negligible contribution of dimerization reaction (1). Hence, the time-dependence expression of $[CH_3CHO]_t$ can be simply approximated to

$$[CH3CHO]t = [CH3CHO]0 exp(-kcomplex(T)[H2O]0t). (VI)$$

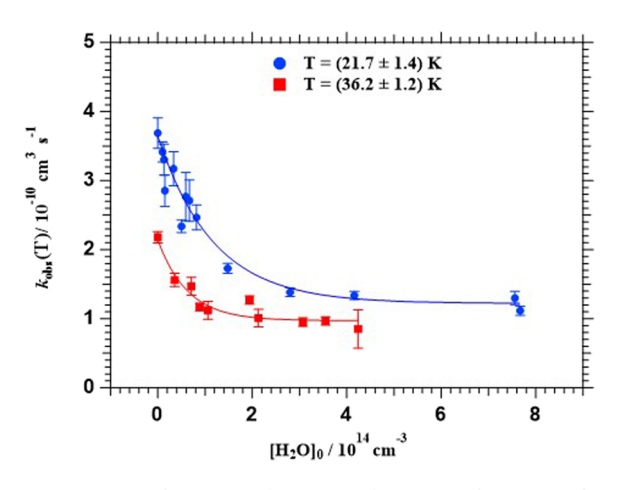
On the other hand, $[CH_3CHO(H_2O)]_t$ can be deduced considering the mass balance for CH_3CHO ,

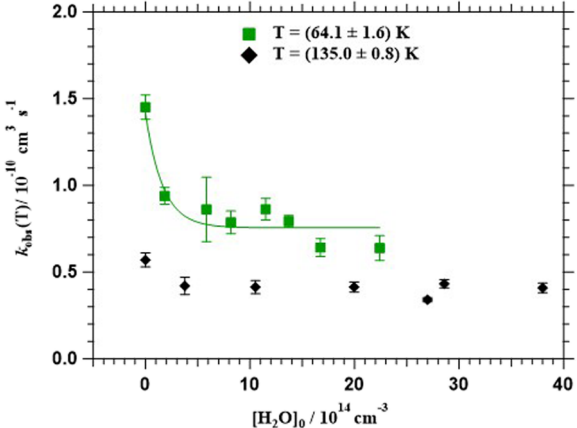
$$[CH3CHO]0 = [CH3CHO]t + [CH3CHO(H2O)]t, (VII)$$

and that the rate of reaction (2) $(k_{complex}(T)[CH_3CHO][H_2O])$ is much higher than that for reaction (3) $(k_{OH_complex}(T)[OH][CH_3CHO(H_2O)])$ since [OH] is always several orders of magnitude smaller than the other involved concentrations. The resulting expression for $[CH_3CHO(H_2O)]_t$ is as follows:

$$\begin{split} \left[\text{CH}_3 \text{CHO}(\text{H}_2 \text{O}) \right]_t &= \left[\text{CH}_3 \text{CHO} \right]_0 \\ &\times \left\{ 1 - \exp \left(-k_{\text{complex}}(\text{T}) \left[\text{H}_2 \text{O} \right]_0 t \right) \right\}. \text{ (VIII)} \end{split}$$

Introducing Eqs. (VI) and (VIII) into Eq. (V) leads to





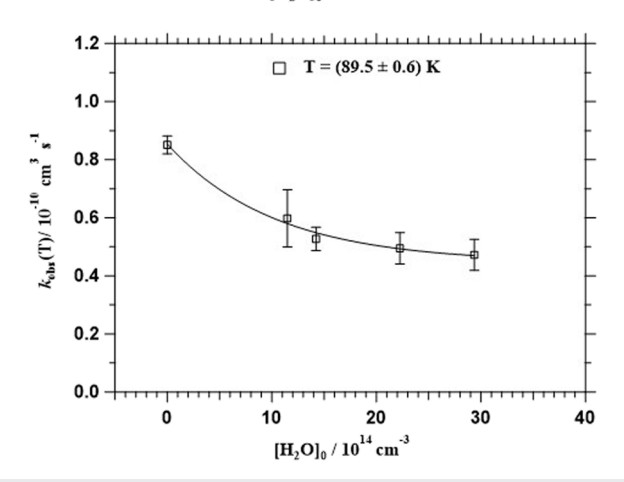


FIG. 5. Dependence of $k_{obs}(T)$ with initial water concentration at different temperatures. The fitting lines represent the obtained result from the fit of the experimental data to Eq. (X). Uncertainties are $\pm 1\sigma$.

$$k' - k'_{0} = [CH_{3}CHO]_{0} \{k_{OH_complex}(T) + \{(k(T) - k_{OH_complex}(T)) \times \exp(-k_{complex}(T)[H_{2}O]_{0}t)\}\}.$$
 (IX)

TABLE IV. Rate coefficients^a for the water-free OH + CH₃CHO reaction [k(T)] and for the water-assisted OH + CH₃CHO reaction $[k_{OH_complex}(T)]$ as a function of temperature.

k(T) (10 ⁻¹⁰ cm ³ s ⁻¹)	$k_{\rm OH_complex}({ m T}) \ (10^{-10} { m cm}^3 { m s}^{-1})$	$k_{\text{OH_complex}}$ (T)/ k (T)
3.69 ± 0.22	1.22 ± 0.11	0.33 ± 0.04
2.18 ± 0.08	0.97 ± 0.06	0.44 ± 0.03
1.45 ± 0.07	0.76 ± 0.05	0.52 ± 0.04
0.85 ± 0.03	0.45 ± 0.03	0.53 ± 0.04
0.58 ± 0.02	0.41 ± 0.03	0.71 ± 0.06
	$\frac{(10^{-10} \text{ cm}^3 \text{ s}^{-1})}{3.69 \pm 0.22}$ 2.18 ± 0.08 1.45 ± 0.07 0.85 ± 0.03	$ \begin{array}{cccc} (10^{-10} \text{ cm}^3 \text{ s}^{-1}) & (10^{-10} \text{ cm}^3 \text{ s}^{-1}) \\ \hline 3.69 \pm 0.22 & 1.22 \pm 0.11 \\ 2.18 \pm 0.08 & 0.97 \pm 0.06 \\ 1.45 \pm 0.07 & 0.76 \pm 0.05 \\ 0.85 \pm 0.03 & 0.45 \pm 0.03 \\ \end{array} $

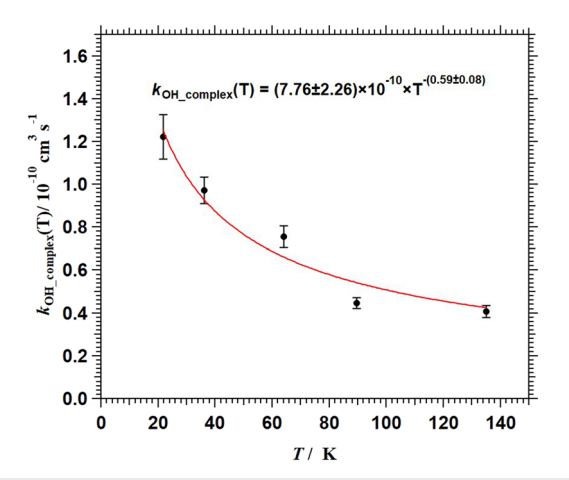
 $[\]frac{\overline{a}}{\pm 1\sigma}$ statistical uncertainties.

Equation (IX) is comparable to Eq. (IV) when time t coincides with the experimental time t_{hydro} used to obtain the OH LIF decays, which allowed for the deduction of the first-order rates $k'-k'_0$ plotted in Fig. 4. As specified earlier, t_{hydro} is the time needed for molecules to flow from the nozzle exit to the extremity of the uniform flow concurring with the detection zone. Note that this time is flow-dependent and its value is given in Table V for each temperature condition employed in this work. From this, the observed rate coefficient can be expressed as

$$k_{\text{obs}}(T) = k_{\text{OH_complex}}(T) + \{ (k(T) - k_{\text{OH_complex}}(T))$$

$$\times \exp(-k_{\text{complex}}(T)[H_2O]_0 t_{\text{hydro}}) \}.$$
 (X)

The $k_{\rm obs}(T)$ vs $[{\rm H_2O}]_0$ curves presented in Fig. 5 are well-described in Eq. (X). Therefore, since k(T) was experimentally obtained in the experiments performed without added water, $k_{\rm complex}(T)$ and $k_{\rm OH_complex}(T)$ were obtained from the fit of $k_{\rm obs}(T)$ vs $[{\rm H_2O}]_0$. Table IV lists the rate coefficient for the water-assisted OH + CH₃CHO reaction and the $k_{\rm OH_complex}(T)/k(T)$ ratios as a function of temperature. Clearly, the reaction of CH₃CHO(H₂O) with OH is slower than the water-free reaction, contrary to the conclusions of Vöhringer-Martinez *et al.* The T-dependence of $k_{\rm OH_complex}(T)$ is well-described by the power relationship, $k_{\rm OH_complex}(T) = AT^n$ in the temperature range 20–135 K (see Fig. 6). The fitted parameters are



 $\label{eq:FIG. 6.} \mbox{FIG. 6. Temperature dependence of the rate coefficient for the OH $+ \mbox{CH}_2\mbox{O}$ (H_2O) reaction, $k_{OH_complex}(T)$.}$

TABLE V. Rate coefficients for the formation of the $CH_3CHO(H_2O)$ complex as $[k_{complex}(T)]$ and the hydrodynamic time as a function of temperature. Uncertainties are $\pm 1\sigma$ statistical errors.

T (K)	t _{hydro} (μs)	$k(T)$ $(10^{-10} \text{ cm}^3 \text{ s}^{-1})$	$k_{\text{complex}}(T)$ (10 ⁻¹¹ cm ³ s ⁻¹)	k_{complex} (T)/ k (T)
21.7 ± 1.4	203	3.69 ± 0.22	4.19 ± 0.54	0.114 ± 0.016
36.2 ± 1.2	278	2.18 ± 0.08	5.72 ± 1.18	0.262 ± 0.055
64.1 ± 1.6	544	1.45 ± 0.07	1.12 ± 0.57	0.077 ± 0.039
89.5 ± 0.6	605	0.85 ± 0.03	0.17 ± 0.03	0.020 ± 0.004
135.0 ± 0.8	239	0.58 ± 0.02		

 $A = (7.8 \pm 2.3) \times 10^{-10} \text{ cm}^3 \text{ s}^{-1}$ and $n = -(0.59 \pm 0.08)$, $\pm 1\sigma$ statistical uncertainties. Regarding the $k_{\text{OH_complex}}(\text{T})/k(\text{T})$ ratio, it slightly increases when temperature increases. In contrast, Iuga *et al.*¹⁷ calculated that the $k_{\text{OH_complex}}(\text{T})/k(\text{T})$ ratio decreases from 0.22 at 220 K to 5.3×10^{-4} at 298 K. Uncertainties in the $k_{\text{OH_complex}}(\text{T})/k(\text{T})$ ratio is the result of the error propagation considering the uncertainties in $k_{\text{OH_complex}}(\text{T})$ and k(T).

Similarly, in Table V, the rate coefficients for the formation of CH₃CHO(H₂O) complex are presented as a function of temperature. As can be seen, at the investigated ultra-low temperatures, the formation of CH₃CHO(H₂O) is around one order of magnitude slower than its reaction with OH radicals. In a general trend, $k_{\text{complex}}(T)$ decreases at high temperatures as the association reactions are less favored. Uncertainties in the $k_{\text{complex}}(T)/k(T)$ ratio is the result of the error propagation considering the uncertainties in $k_{\text{complex}}(T)$ and k(T).

V. THEORETICAL RESULTS AND DISCUSSION

A. Equilibrium constants for the $CH_3CHO(H_2O)$ and $(CH_3CHO)_2$ complexes

Two geometries were found for the $CH_3CHO(H_2O)$ complex (see Fig. S1 of the supplementary material). The most stable, at $-4.77~\rm kcal~mol^{-1}$ below the reactants, has the H_2O molecule spanning the CH_3 and acetyl O-atom, while the other complex, at $-4.21~\rm kcal~mol^{-1}$, bridges the CHO oxygen and the H-atom. The equilibrium constant was calculated to be $K_{eq}(20-300~\rm K)=6.19\times 10^{-26}~\rm (T/K)^{0.19}~\rm exp(2488~\rm K/T)~\rm cm^3~molecule^{-1}$, i.e., $K_{eq}(100~\rm K)=8.7\times 10^{-15}~\rm cm^3~molecule^{-1}$ (see Fig. 7). Even at room temperature, the side-way complex contributes 88% of the complex population, and at the low temperatures in the experiments, the complex will exist near-exclusively of this lowest-energy complex. The low equilibrium constant near room temperature reconfirms earlier reports 17,54 that water complexation cannot effectively catalyze acetaldehyde oxidation by OH in an atmospheric setting due to the low incidence of H_2O -complexed CH_3CHO .

For the $(CH_3CHO)_2$ complex, eight geometries were found, ranging stability from -4.3 to -1.8 kcal mol^{-1} below the free constituents (see Fig. S1 of the supplementary material). The most stable geometry is best described as an L-shaped structure, with the two acetaldehydes interacting with their aldehyde groups. The equilibrium constant was calculated to be $K_{eq}(20-300 \text{ K}) = 7.30 \times 10^{-31} \text{ (T/K)}^{1.94} \text{ exp}(2305 \text{ K/T) cm}^3 \text{ molecule}^{-1}$, i.e., $K_{eq}(100 \text{ K}) = 4.9 \times 10^{-17} \text{ cm}^3 \text{ molecule}^{-1}$. As seen in Fig. 7, the equilibrium

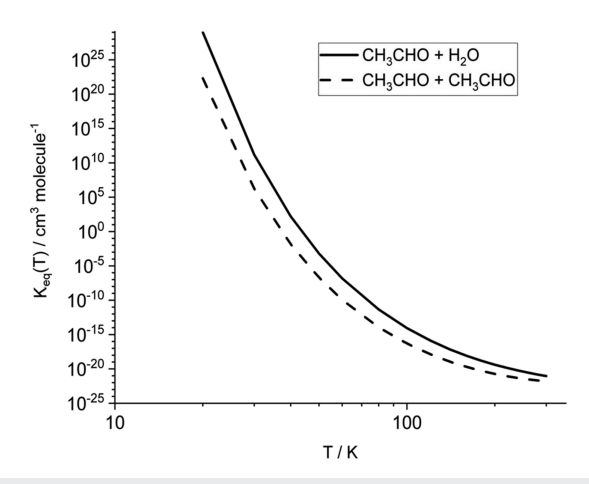


FIG. 7. Equilibrium constants for the CH₃CHO(H₂O) and (CH₃CHO)₂ complexes.

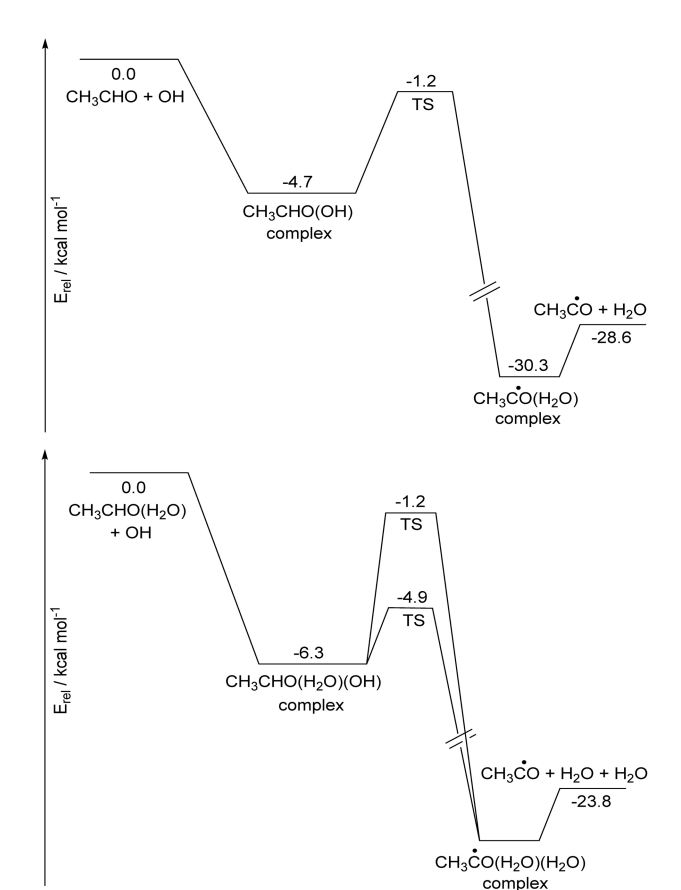
constant for the water complex is higher by at least one order of magnitude, and typically more, across the experimentally relevant temperatures. The preference for the water complex is driven both by its deeper energy well and by the entropic advantage of complexing a water molecule (low quantum state density for relative translation and rotation) compared to a CH₃CHO molecule (high state density). The higher equilibrium constant for H₂O implies that adding water to the reaction mixture will displace acetaldehyde from its dimer complexes and preferentially, if not exclusively, form water + acetaldehyde complexes.

B. Potential energy surfaces (PESs)

1. PES for the CH3CHO + OH system

Figure 8 shows the potential energy surfaces (PESs) for the reaction of OH radicals with CH $_3$ CHO, which initially proceeds by the formation of a pre-reactive complex, for which five stable minima were found, with energies ranging from -4.7 to -0.1 kcal mol $^{-1}$ below the free reactants (see Fig. S2 of the supplementary material). The most stable complex geometry has the OH radical bridging the acetaldehyde O-atom and the CH $_3$ group, whereas the second-most stable complex, only 0.71 kcal mol $^{-1}$ higher in energy, complexes the OH radical across the CHO group. The remaining complexes are much less stable, >3 kcal mol $^{-1}$ above the most stable complex, and correspond to van der Waals complexes without an H-bond. Figure SI-10 presents the energies and ball-and-stick depiction of the geometries of the complexes and transition states in the CH $_3$ CHO + OH system.

The H-abstraction pathway involves two near-isoenergetic submerged transition states at -1.19 and -1.15 kcal mol⁻¹ below the free reactants. Our level of theory thus predicts a higher-energy barrier than those in the works of Vöhringer-Martinez *et al.*²² (-2.4 kcal mol⁻¹) and Iuga *et al.*¹⁷ (-1.28 and -1.72 kcal mol⁻¹). The lowest-energy pathway has a slightly non-planar transition state (TS) geometry, and intrinsic reaction coordinate (IRC) calculations show that it starts at the second-most stable H-bonded pre-reaction complex. The second TS geometry is fully planar, and its pathway initiates at a van der Waals reactant complex. We note that it is sometimes thought that the TS is submerged due to the pre-reaction H-bonding



 $\label{eq:FIG. 8. ZPE-corrected potential energy surface for the CH_3CHO + OH and CH_3CHO(H_2O) + OH reaction systems at the $CCSD(T)/aug-cc-pVTZ/M06-2X-D3/aug-cc-pVTZ level of theory.}$

between the carbonyl group and the OH radical. In the TS geometries, however, the H-bond is fully broken, with $^{\bullet}$ OH-O=C distances of \sim 3.8 Å, and the submergence is due to van der Waals and dipole interactions.

Once the TS threshold is traversed, the reaction products, $CH_3CO + H_2O$, first form a post-reaction complex, for which we located three stable geometries at energies ranging from -32.0 to 30.3 kcal mol^{-1} (see Fig. S2 of the supplementary material). This complex readily dissociates to the free products at an energy of -28.6 kcal mol^{-1} .

The potential energy surface found here has the same essential features as determined in earlier theoretical works, ^{17,22,55–57} and any difference can be attributed to our more detailed characterization of the complexation properties at a higher level of theory.

2. PES of the OH + $CH_3CHO(H_2O)$ system

Figure 8 also shows the PES for the reaction of OH radicals with the $CH_3CHO(H_2O)$ complex; as already indicated, this reactant complex has two possible geometries, the most stable of which has the H_2O molecule complexed to the side of CH_3CHO . Adding OH allows for many distinct $CH_3CHO(H_2O)(OH)$ complexes, where we have located 15 stable geometries spanning 5.6 kcal mol^{-1} in

relative energies, with the energetically lowest at -6.3 kcal mol^{-1} below the reactants. In Fig. S3 of the supplementary material, the energies and ball-and-stick depiction of the geometries of the complexes and transition states in the $\mathrm{CH_3CHO}(\mathrm{H_2O})$ + OH system are shown.

Two H-abstraction transition states were found, each with a pathway starting at a distinct $CH_3CHO(H_2O)$ complex. The lowest-energy transition state, $-4.9 \, \text{kcal mol}^{-1}$ below the reactants, connects the OH radical, the H_2O molecule, and the aldehyde –CHO moiety in an H-bonded seven-membered ring. This barrier height is less submerged than found earlier by Vöhringer-Martinez *et al.*²² ($-6.3 \, \text{kcal mol}^{-1}$) and Iuga *et al.*¹⁷ ($-8.8 \, \text{and} \, -9.5 \, \text{kcal mol}^{-1}$). The geometry of the other TS resembles the $CH_3CHO + OH \, \text{transition}$ state, but with a spectator H_2O molecule complexed on the side of CH_3CHO between the carbonyl O-atom and the methyl group; this TS is 3.72 kcal mol^{-1} above the lower TS owing to the absence of an H-bond on the abstracting OH radical, as in the $CH_3CHO + OH \, \text{PES}$. Once the TS is traversed, the reaction products, $CH_3CO + 2 \, H_2O$, first form a post-reaction complex, which readily dissociates to the free products at an energy of $-23.8 \, \text{kcal mol}^{-1}$.

C. Comparison of the reaction dynamics without and with $\mbox{H}_2\mbox{O}$

It is possible, in principle, to theoretically predict the temperature- and pressure-dependent rate coefficients for the $\mathrm{CH_3CHO} + \mathrm{OH}$ and $\mathrm{CH_3CHO} + \mathrm{H_2O} + \mathrm{OH}$ reaction systems; we refer to our earlier work on $\mathrm{CH_3OH} + \mathrm{OH}$ on the methodologies involved. Such rate coefficient calculations are typically accurate to a factor of 2–4, which, in this case, is unfortunately insufficient to discriminate between the reaction rate coefficients of the cases with and without water. As such, we have not performed these costly theoretical kinetic calculations. The available data, however, are still able to reveal interesting details on the reaction dynamics and the effect of an $\mathrm{H_2O}$ catalyst.

1. Reaction dynamics of H-abstraction

The reaction of CH₃CHO + OH is fast owing to its submerged H-abstraction TS. Its rate coefficient k(T) has a negative temperature dependence, which is caused by two effects. First, the initial complexation reaction is a barrierless reaction, which is known to show a slight negative temperature dependence. Second, at higher temperatures, the H-abstraction TS faces more competition from the energetically higher, but entropically more favorable redissociation of the complexes to the free reactants due to the increased energy in the nascent complexes, thus reducing the product formation efficiency of the overall reaction. This latter competition is more effective in the low-pressure regime when the complexes formed do not lose energy in collisions with the bath gas, and thus, all have sufficient energy for redissociation. At high pressure, the complexes are, instead, thermalized within the pre-reaction complex energy well and typically have insufficient energy to redissociate, leaving only Habstraction as a viable reaction path, be it over the submerged barrier or by tunneling through this barrier.

2. The impact of water complexation

Comparing the potential energy surface with added water against that without a water molecule suggests, at first sight, that the $\text{CH}_3\text{CHO}(\text{H}_2\text{O})$ + OH reaction should be the faster reaction. First, the pre-reaction complexes are more stable, and there are more

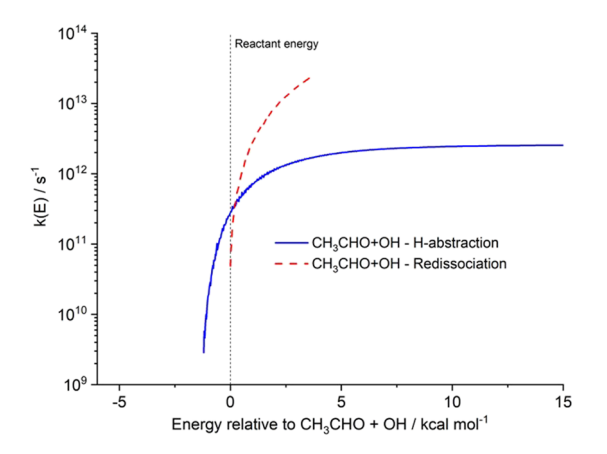
complexation geometries possible, which typically leads to faster complexation. Furthermore, the H-abstraction TS is greatly reduced in energy, facilitating the H-abstraction and reducing redissociation of the complexes to the reactants. A more detailed comparison, however, reveals some surprising effects.

First, the dipole moment of the CH₃CHO(H₂O) complex, 1.9 or 2.1 D depending on the complex geometry, is significantly smaller than that of the free CH₃CHO molecule, 2.9 D. The attractive force exerted on the OH radical at long distances is thus less for the water complex, leading to a lower capture rate. This long-range interaction is important mostly at the lowest temperatures, as there the energies are lowest and the entropic bottleneck is located at the furthest distances. At higher energies, the kinetic bottleneck along the barrierless complexation pathway will tighten, shifting it to closer separations where the improved H-bonding synergies within the deeper water-complex energy well can be more effective. As already mentioned, we cannot theoretically quantify with sufficient accuracy to what internal energy the capture rate for the water complex will remain below that of the free CH₃CHO reactant.

A second surprising observation is that H-abstraction from CH₃CHO(H₂O) is not all that favorable, despite the lowered barrier height. Specifically, the lowest abstraction TS has multiple H-bonds in a ring structure, making this TS very rigid and thus entropically unfavorable. To illustrate, we mention that for a Boltzmann distribution of the complexes at 300 K, the higher H-abstraction TS already contributes ~25% of the reaction flux, despite having a Boltzmann energy factor that is 620 times less favorable (3.72 kcal mol⁻¹ above the lowest TS). In the high-pressure regime, the lowest TS will remain the dominant pathway as the complexes are stabilized into the bottom of the energy well. In the low-pressure regime, however, the complexes retain the full energy content of the reaction, and the reaction rate is no longer energy-limited but instead controlled by the unfavorable entropy, preventing the anticipated acceleration of H-abstraction. This is illustrated in Fig. 9, showing the energyspecific rate coefficients for H-abstraction for the water-containing complexes, calculated using RRKM theory, including all conformers of reactants and transition states. The rate coefficient k(E) through the lowest TS reaches a maximum at internal CH₃CHO(H₂O)(OH) energies even less than those received in its formation and reduces slightly at higher energies due to the faster increase in the state density of the many pre-reaction complexes compared to the TS. This is in stark contrast to the energy-specific rates intuitively expected when assuming similar rigidity for all TS structure. We illustrate this in Fig. 9 or a hypothetical TS at the same energy as the low TS, but entropically as loose as the high TS or as the CH₃CHO + OH TS; this hypothetical case leads to very fast H-abstraction rates. In reality, then, the nascent complexes may not necessarily always undergo H-abstraction despite the lower-energy TS, and redissociation to the reactants should be considered. At increasing internal energies, the less rigid higher-energy H-abstraction TS increases in importance and finally carries the largest reaction flux. The energyspecific k(E) for the water-free complexes are higher due to the lower state density for the CH₃CHO(OH) complexes compared to the $CH_3CHO(H_2O)(OH)$ complexes.

3. Non-reactive redissociation of the OH complexes

To judge the impact of redissociation on effective product formation, we need to estimate the redissociation reaction rate



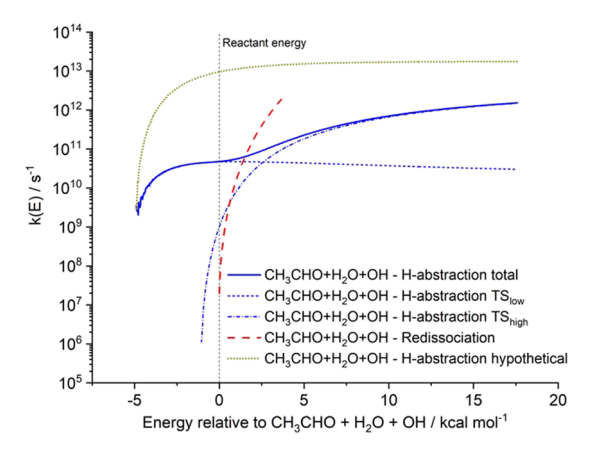


FIG. 9. Energy-specific rate coefficients for H-abstraction and redissociation in the pre-reaction complexes of the $CH_3CHO + OH$ and $CH_3CHO(H_2O) + OH$ reactions. H-abstraction rates are calculated directly from the quantum chemical data, while redissociation is estimated by inversion of the forward reaction rate using the equilibrium constant. The hypothetical transition state for H-abstraction is based on an intuitive interpretation of the PES, ignoring the impact of entropy (see the text).

coefficients. Directly predicting the redissociation rates would require characterizing the barrierless pathways for all approaches to all complexes, which is computationally very costly. Furthermore, as already mentioned, the expected accuracy of the predictions would not be sufficient to unequivocally support the experimental observation that the rate coefficient is reduced by a factor of two in the case of added water. Still, to show that redissociation rate coefficients are in the correct order of magnitude, we should roughly estimate whether the entropic advantage of the redissociation is sufficient to overcome the 4.9 kcal mol⁻¹ energetic advantage of H-abstraction.

The redissociation rate coefficients can be estimated starting from the temperature-dependent equilibrium constants for OH-complexes. We find $K_{\text{CH}_3\text{CHO}+\text{OH}}(T) = 2.53 \times 10^{-25}~T^{-0.10}$ exp(2456 K/T) and $K_{\text{CH}_3\text{CHO}-\text{H2O}+\text{OH}}(T) = 2.31 \times 10^{-27}~T^{0.47}$ exp(3302 K/T). Given that an equilibrium constant equals the ratio of the rate coefficients for the forward and reverse reactions, relying on the transition state theory expression for k(T), and assuming a

rate coefficient of complexation $k_{complexation}(T)$ similar to the experimental rate coefficient of $\sim 3 \times 10^{-10}$ cm³ molecule⁻¹ s⁻¹, we can then derive the T-dependent partition functions $Q_{TS}(T)$ for the barrierless complexation/redissociation TS,

$$K_{eq}(T) = \frac{k_{complexation}(T)}{k_{redissociation}(T)},$$
 (XI)

$$\begin{aligned} k_{redissociation}(\mathrm{T}) &= \frac{k_{complexation}(\mathrm{T})}{K_{eq}(\mathrm{T})} \\ &= \frac{kT}{h} \frac{Q_{TS}(\mathrm{T})}{Q_{\mathrm{complex}}(\mathrm{T})} \exp\left(\frac{-E_b}{kT}\right). \end{aligned} \tag{XII}$$

We can then obtain k(E) for redissociation, where we integrate $N_{TS}(E)$ over energies 0 to E to obtain the sum of states $G_{TS}(E)$, and use the density of states $N_{\text{complex}}(E)$ calculated for the ensemble of complexes using the Beyer-Swinehart-Stein-Rabinovitch algorithm. The resulting semi-quantitative k(E) for redissociation are highly approximate, with an anticipated uncertainty of an order of magnitude. They can be compared to the more reliable rate coefficient for H-abstraction, where we find that even for the hydrated case redissociation reaches parity with the H-abstraction rate coefficients with only ~2 kcal mol⁻¹ excess energy in the reactants (see Fig. 9), and within the uncertainty, redissociation is competitive against product formation. This is a counter-intuitive result as one would normally not assume the H-abstraction TS to be so entropically hindered. Indeed, a hypothetical TS ignoring the rigidity of the lowest TS would not allow for redissociation at all, as also illustrated in Fig. 9. Given the large uncertainty, we refrain from quantifying the fraction of redissociation but conclude only that redissociation should not be discounted even in the water-catalyzed reaction despite the (deeply) submerged TS. The CH₃CHO(H₂O)(OH) complex can also dissociate to CH₃CHO(OH) + H₂O; this is isoenergetic to the OH loss, but as the cold CH₃CHO-OH complex formed will then undergo H-abstraction by tunneling, this channel does not decrease the effective rate coefficient for product formation.

A critical condition of the above analysis is that the OH-complexes retain the full nascent energy of the reaction. As shown in Fig. 9, the energy-specific rates k(E) for dissociation are comparatively high in both systems, $\ge 4 \times 10^{10} \, \mathrm{s}^{-1}$ even for the water complex. Hence, in the experimental conditions, both reactions are in the *low-pressure regime*, and even at 1 atm, the reactions will still be in the low-pressure (CH₃CHO + OH) or fall-off regime [CH₃CHO(H₂O) + OH].

4. Temperature dependence of effective product formation

The experimental data do not reveal which of the above two mechanistic effects, i.e., lower capture rate at low energies due to lower dipole moment, vs redissociation to the reactants due to the entropy of the H-abstraction TS, is the cause of the lower rate coefficient for CH₃CHO(H₂O) compared to CH₃CHO. The measurements do indicate that the redissociation fraction cannot be very high at the lowest temperatures as otherwise the rate coefficient would drop well below the collision limit, in disagreement with the observations. The experimentally observed decrease in the difference between the two cases with increasing temperature, starting at factor

3 at 21 K and disappearing above 135 K, could have several reasons. First, the difference in the capture rate between the two systems could decrease, as for higher energies, the rate of reaction through barrierless complexation channels is determined increasingly by the OH-complex properties, and the effect on the long-range capture by the lower dipole moment of CH₃CHO(H₂O) compared to CH₃CHO would become less important. Second, the availability of a second H-abstraction channel in the CH₃CHO(H₂O)(OH) complex increases the total product formation rate at increasing internal energies faster than for CH₃CHO + OH (see Fig. 9). Higher temperatures could then allow the water complex to have a higher ratio of product formation to redissociation than the water-free reaction, increasing its apparent reaction rate. Likely, the observed trend is caused by a combination of these mechanisms. In principle, it should be possible to separate the effects by measurements in lowtemperature but high-pressure gas-phase conditions, but we are not aware of an experimental setup that is capable of performing such measurements.

VI. CONCLUSIONS

In conclusion, we report that there is an anti-catalytic effect of water on the OH + CH₃CHO reaction at ultra-low temperatures (T = 21.7-135.0 K). Increasing the water content in the jet converts, to a great extent, "free" CH₃CHO into a CH₃CHO(H₂O) complex, which enables us to measure the impact of H₂O on its OH-rate coefficient in that temperature range. Our experimental results show that the water-assisted reaction is slower than the OH + CH₃CHO reaction at low temperatures by a factor of ~3 at 21.7 K and ~2 at 36.2-89.5 K, while almost no effect of added H₂O was observed at 135.0 K. In agreement with the work of Vöhringer-Martinez et al., 22 our theoretical calculations find that complexation of CH₃CHO with H₂O reduces the barrier to H-abstraction by 3.7 kcal mol⁻¹. The above experimental results thus appear in disagreement with the theoretical analysis, as intuitively one would, instead, expect a rate increase. However, the lower dipole moment of the CH₃CHO(H₂O) complex compared to free CH₃CHO reduces the long-range attraction to OH radicals, lowering the rate coefficient, especially for the studied low temperatures where the rate is driven by long-range interaction. Furthermore, the hydrogen bonding with water strongly disadvantages the H-abstraction entropically. At the pressures used in the experiments (0.42-5.55 mbar), the nascent OH-complexes retain their full internal energy, and the entropic hindrance slows down the water-complexed reaction at those energies sufficiently to allow for non-reactive redissociation toward the reactants to remain competitive against H-abstraction, to the same extent as for the water-free reaction.

The slight positive catalytic effect of a factor of ~2 previously described by Vohringer-Martinez *et al.* for the title reaction 22 is attributed to a bias in these earlier measurements due to the short hydrodynamic time and high initial concentrations of CH₃CHO, which favors the formation of acetaldehyde dimers, which have a lower reaction rate toward OH. We find that between 20 and 90 K, the formation of CH₃CHO(H₂O) is more favorable than (CH₃CHO)₂ and the present study provides an estimation of the association rate coefficient for the hydrated complex formation and of the rate coefficient for the OH + CH₃CHO(H₂O) reaction in this temperature range.

SUPPLEMENTARY MATERIAL

See the supplementary material for energies and geometries of the CH₃CHO(H₂O) and (CH₃CHO)₂ complexes.

ACKNOWLEDGMENTS

The authors thank Professor Claus J. Nielsen for his help in the quantification of the water content by IR spectroscopy. This work was partially supported by the NANOCOSMOS (Grant No. SyG-610256, European Research Council) project and UCLM (Ayudas para la financiación de actividades de investigación dirigidas a grupos REF: 01110G0138). M.A. and S.B. would like to acknowledge UCLM for funding their contracts through the Plan Propio de Investigación. A.C. is also grateful to the French National Programme "Physique et Chimie du Milieu Interstellaire" (PCMI) of CNRS/INSU with INC/INP co-funded by CEA and CNES for constant support.

DATA AVAILABILITY

The data that support the findings of this study are available within the article and its supplementary material.

REFERENCES

- ¹L. Paganini, G. L. Villanueva, L. Roth, A. M. Mandell, T. A. Hurford, K. D. Retherford, and M. J. Mumma, Nat. Astron. 4, 266 (2020).
- ²Y. Dong, T. W. Hill, B. D. Teolis, B. A. Magee, and J. H. Waite, J. Geophys. Res.: Space Phys. **116**, A10204, https://doi.org/10.1029/2011ja016693 (2011).
- V. Cottini, C. A. Nixon, D. E. Jennings, C. M. Anderson, N. Gorius, G. L. Bjoraker, A. Coustenis, N. A. Teanby, R. K. Achterberg, B. Bézard, R. de Kok, E. Lellouch, P. G. J. Irwin, F. M. Flasar, and G. Bampasidis, Icarus 220, 855 (2012).
 N. Flagey, P. F. Goldsmith, D. C. Lis, M. Gerin, D. Neufeld, P. Sonnentrucker, M. De Luca, B. Godard, J. R. Goicoechea, R. Monje, and T. G. Phillips, Astrophys. J. 762, 11 (2013).
- ⁵E. F. Van Dishoeck, E. Herbst, and D. A. Neufeld, Chem. Rev. 113, 9043 (2013).
 ⁶M. J. Mumma, H. A. Weaver, H. P. Larson, D. S. Davis, and M. Williams, Science 232, 1523 (1986).
- Weinreb, A. H. Barrett, M. L. Meeks, and J. C. Henry, Nature 200, 829 (1963).
 J. Crovisier, P. Colom, E. Gérard, D. Bockelée-Morvan, and G. Bourgois, Astron. Astrophys. 393, 1053 (2002).
- ⁹Z. Wang, X. Chen, F. Gao, S. Zhang, X.-W. Zheng, W.-H. Ip, N. Wang, X. Liu, X.-T. Zuo, W. Gou, and S.-Q. Chang, Astron. J. **154**, 249 (2017).
- ¹⁰N. Biver and D. Bockelée-Morvan, ACS Earth Space Chem. 3, 1550 (2019).
- ¹¹C. A. Gottlieb, in *Molecules in the Galactic Environment*, edited by M. A. Gordon and L. E. Snyder (Wiley-Interscience New York, 1973), p. 181.
- ¹² M. Schuhmann, K. Altwegg, H. Balsiger, J.-J. Berthelier, J. De Keyser, S. A. Fuselier, S. Gasc, T. I. Gombosi, N. Hänni, M. Rubin, T. Sémon, C.-Y. Tzou, and S. F. Wampfler, ACS Earth Space Chem. 3, 1854 (2019).
- ¹³V. Thiel, A. Belloche, K. M. Menten, R. T. Garrod, and H. S. P. Müller, Astron. Astrophys. **605**, L6 (2017).
- ¹⁴J. M. Anglada and J. Gonzalez, ChemPhysChem 10, 3034 (2009).
- ¹⁵C. Iuga, J. R. Alvarez-Idaboy, and A. Vivier-Bunge, Chem. Phys. Lett. 501, 11 (2010).
- ¹⁶C. Iuga, J. R. Alvarez-Idaboy, and A. Vivier-Bunge, Theor. Chem. Acc. 129, 209 (2011).
- ¹⁷C. Iuga, J. R. Alvarez-Idaboy, L. Reyes, and A. Vivier-Bunge, J. Phys. Chem. Lett. 1, 3112 (2010).
- ¹⁸ M. A. Allodi, M. E. Dunn, J. Livada, K. N. Kirschner, and G. C. Shields, J. Phys. Chem. A **110**, 13283 (2006).
- ¹⁹L. Xu, N. T. Tsona, S. Tang, J. Li, and L. Du, ACS Omega 4, 5805 (2019).

- ²⁰W. Chao, J. Jr-Min Lin, K. Takahashi, A. Tomas, L. Yu, Y. Kajii, S. Batut, C. Schoemaecker, and C. Fittschen, Angew. Chem., Int. Ed. 58, 5013 (2019).
- ²¹ J. Wu, L. G. Gao, Z. Varga, X. Xu, W. Ren, and D. G. Truhlar, Angew. Chem., Int. Ed. **59**, 10826 (2020).
- ²² E. Vöhringer-Martinez, B. Hansmann, H. Hernandez, J. S. Francisco, J. Troe, and B. Abel, Science 315, 497 (2007).
- ²³ R. A. Jara-Toro, F. J. Hernández, R. A. Taccone, S. I. Lane, and G. A. Pino, Angew. Chem., Int. Ed. 56, 2166 (2017).
- ²⁴ R. A. Jara-Toro, F. J. Hernández, M. D. L. A. Garavagno, R. A. Taccone, and G. A. Pino, Phys. Chem. Chem. Phys. **20**, 27885 (2018).
- ²⁵I. Weber, H. Bouzidi, B. Krumm, C. Schoemaecker, A. Tomas, and C. Fittschen, Phys. Chem. Chem. Phys. **22**, 7165 (2020).
- ²⁶ E. Vöhringer-Martinez, E. Tellbach, M. Liessmann, and B. Abel, J. Phys. Chem. A 114, 9720 (2010).
- ²⁷I. Smith, Science **315**, 470 (2007).
- ²⁸ E. Jiménez, B. Ballesteros, A. Canosa, T. M. Townsend, F. J. Maigler, V. Napal, B. R. Rowe, and J. Albaladejo, Rev. Sci. Instrum. 86, 045108 (2015).
- ²⁹ A. Canosa, A. J. Ocaña, M. Antiñolo, B. Ballesteros, E. Jiménez, and J. Albaladejo, Exp. Fluids 57, 152 (2016).
- ³⁰ A. J. Ocaña, S. Blázquez, B. Ballesteros, A. Canosa, M. Antiñolo, J. Albaladejo, and E. Jiménez, Phys. Chem. Chem. Phys. 20, 5865 (2018).
- ³¹ A. J. Ocaña, S. Blázquez, A. Potapov, B. Ballesteros, A. Canosa, M. Antiñolo, L. Vereecken, J. Albaladejo, and E. Jiménez, Phys. Chem. Chem. Phys. 21, 6942 (2019).
- ³² S. Blázquez, D. González, E. M. Neeman, B. Ballesteros, M. Agúndez, A. Canosa, J. Albaladejo, J. Cernicharo, and E. Jiménez, Phys. Chem. Chem. Phys. 22, 20562 (2020).
- ³³ J. B. Burkholder, S. P. Sander, J. P. D. Abbatt, J. R. Barker, R. E. Huie, C. E. Kolb, M. J. Kurylo, V. L. Orkin, D. M. Wilmouth, and P. H. Wine, Chemical Kinetics and Photochemical Data for Use in Atmospheric Studies: Evaluation Number 18, Publication 15-10, Jet Propulsion Laboratory, National Aeronautics and Space Administration, Pasadena, 2015.
- ³⁴ A. J. Ocaña, E. Jiménez, B. Ballesteros, A. Canosa, M. Antiñolo, J. Albaladejo, M. Agúndez, J. Cernicharo, A. Zanchet, P. del Mazo, O. Roncero, and A. Aguado, Astrophys. J. 850, 28 (2017).
- ³⁵M. Antiñolo, A. J. Ocaña, J. P. Aranguren, S. I. Lane, J. Albaladejo, and E. Jiménez, Chemosphere 181, 232 (2017).
- ³⁶S. Blázquez, M. Antiñolo, O. J. Nielsen, J. Albaladejo, and E. Jiménez, Chem. Phys. Lett. 687, 297 (2017).
- ³⁷E. Jiménez, B. Lanza, A. Garzón, B. Ballesteros, and J. Albaladejo, J. Phys. Chem. A 109, 10903 (2005).
- ³⁸M. Antiñolo, E. Jiménez, A. Notario, E. Martínez, and J. Albaladejo, Atmos. Chem. Phys. 10, 1911 (2010).
- ³⁹D. W. T. Griffith, N. M. Deutscher, C. Caldow, G. Kettlewell, M. Riggenbach, and S. Hammer, Atmos. Meas. Tech. 5, 2481 (2012).
- ⁴⁰D. W. T. Griffith, Appl. Spectrosc. **50**, 59 (1996).

- ⁴¹ L. S. Rothman, I. E. Gordon, A. Barbe, D. C. Benner, P. F. Bernath, M. Birk, V. Boudon, L. R. Brown, A. Campargue, J.-P. Champion, K. Chance, L. H. Coudert, V. Dana, V. M. Devi, S. Fally, J.-M. Flaud, R. R. Gamache, A. Goldman, D. Jacquemart, I. Kleiner, N. Lacome, W. J. Lafferty, J.-Y. Mandin, S. T. Massie, S. N. Mikhailenko, C. E. Miller, N. Moazzen-Ahmadi, O. V. Naumenko, A. V. Nikitin, J. Orphal, V. I. Perevalov, A. Perrin, A. Predoi-Cross, C. P. Rinsland, M. Rotger, M. Šimečková, M. A. H. Smith, K. Sung, S. A. Tashkun, J. Tennyson, R. A. Toth, A. C. Vandaele, and J. Vander Auwera, J. Quant. Spectrosc. Radiat. Transfer 110, 533 (2009).
- 42 Y. Zhao and D. G. Truhlar, Theor. Chem. Acc. 120, 215 (2008).
- ⁴³T. H. Dunning, J. Chem. Phys. **90**, 1007 (1989).
- ⁴⁴W. Hujo and S. Grimme, Phys. Chem. Chem. Phys. 13, 13942 (2011).
- ⁴⁵S. Grimme, S. Ehrlich, and L. Goerigk, J. Comput. Chem. **32**, 1456 (2011).
- ⁴⁶G. D. Purvis and R. J. Bartlett, J. Chem. Phys. **76**, 1910 (1982).
- ⁴⁷I. M. Alecu, J. Zheng, Y. Zhao, and D. G. Truhlar, J. Chem. Theory Comput. 6, 2872 (2010).
- ⁴⁸L. Vereecken, G. Huyberechts, and J. Peeters, J. Chem. Phys. **106**, 6564 (1997).
- ⁴⁹D. G. Truhlar, B. C. Garrett, and S. J. Klippenstein, J. Phys. Chem. **100**, 12771 (1996).
- ⁵⁰ K. Holbrook, M. J. Pilling, and S. H. Robertson, *Unimolecular Reactions*, 2nd ed. (1996).
- ⁵¹ P. J. Rob-inson, K. A. Holbrook, A. W. Snyder, and D. John Mitchell, *Theory of Unimolecular and Recombination Reactions* (Blackwell Scientific Publications, Oxfordshire, UK, 1992).
- ⁵² M. J. Frisch, G. W. Trucks, H. B. Schlegel, G. E. Scuseria, M. A. Robb, J. R. Cheeseman, G. Scalmani, V. Barone, G. A. Petersson, H. Nakatsuji, X. Li, M. Caricato, A. V. Marenich, J. Bloino, B. G. Janesko, R. Gomperts, B. Mennucci, H. P. Hratchian, J. V. Ortiz, A. F. Izmaylov, J. L. Sonnenberg, D. Williams-Young, F. Ding, F. Lipparini, F. Egidi, J. Goings, B. Peng, A. Petrone, T. Henderson, D. Ranasinghe, V. G. Zakrzewski, J. Gao, N. Rega, G. Zheng, W. Liang, M. Hada, M. Ehara, K. Toyota, R. Fukuda, J. Hasegawa, M. Ishida, T. Nakajima, Y. Honda, O. Kitao, H. Nakai, T. Vreven, K. Throssell, J. A. Montgomery, J. E. Peralta, F. Ogliaro, M. J. Bearpark, J. J. Heyd, E. N. Brothers, K. N. Kudin, V. N. Staroverov, T. A. Keith, R. Kobayashi, J. Normand, K. Raghavachari, A. P. Rendell, J. C. Burant, S. S. Iyengar, J. Tomasi, M. Cossi, J. M. Millam, M. Klene, C. Adamo, R. Cammi, J. W. Ochterski, R. L. Martin, K. Morokuma, O. Farkas, J. B. Foresman, and D. J. Fox, Gaussian, Inc., Wallingford, CT, 2016.
- ⁵³R. J. Shannon, J. C. Gómez Martín, R. L. Caravan, M. A. Blitz, J. M. C. Plane, D. E. Heard, M. Antiñolo, M. Agúndez, E. Jiménez, B. Ballesteros, A. Canosa, G. El Dib, J. Albaladejo, and J. Cernicharo, Phys. Chem. Chem. Phys. 20, 8349 (2018).
- ⁵⁴D. L. Thomsen, T. Kurtén, S. Jørgensen, T. J. Wallington, S. B. Baggesen, C. Aalling, and H. G. Kjaergaard, Phys. Chem. Chem. Phys. 14, 12992 (2012).
- ⁵⁵J. Mendes, C.-W. Zhou, and H. J. Curran, J. Phys. Chem. A **118**, 12089 (2014).
- ⁵⁶J. R. Alvarez-Idaboy, N. Mora-Diez, R. J. Boyd, and A. Vivier-Bunge, J. Am. Chem. Soc. **123**, 2018 (2001).
- ⁵⁷ M. Li, J.-S. Zhang, W. Shen, and Q.-X. Meng, Chin. J. Chem. **22**, 792 (2004).